Continuum Mech. Thermodyn. (2017) 29:1135–1148
DOI 10.1007/s00161-017-0562-1

ORIGINAL ARTICLE

Matthias Wunde · Manfred Klüppel

Impact of mixing procedure on phase morphology and fracture mechanical properties of carbon black-filled NR/SBR blends

Received: 30 September 2016 / Accepted: 7 March 2017 / Published online: 30 March 2017

Abstract Based on a viscoelastic model, the filler distribution and the amount of interphase of carbon black-filled blends of natural rubber (NR) with styrene-butadiene rubber (SBR) are evaluated. Hereby, the total dissipated energy G'' during dynamical straining is decomposed into the contributions of the different polymer phases and the interphase. For the NR/SBR blends, we find a higher filling of the SBR phase and the interphase and a lower filling of the NR phase. The filler distribution itself depends not only on the affinity of the polymer to the filler but also on the mixing procedure. This is investigated by studying NR/SBR blends prepared by two different mixing procedures. In the standard mixing procedure, the polymers are mixed first, and then, the filler is added. In the batch mixing procedure, the filler is previously mixed in the NR only and then blended with SBR. Batch mixing is resulting in an increase in the filling of the interphase due to filler transfer from NR to SBR. The results for the filler distribution are compared to fatigue crack propagation rates under pulsed excitation. The crack propagation is accelerated when substituting NR with SBR. The batched samples show higher crack propagation rates at higher tearing energies due to a worse dispersion of the carbon black and/or higher filler loading of the interphase.

Keywords Filled rubber blends · Filler distribution · Phase morphology · Interphase · Fracture mechanics · Viscoelastic model

1 Introduction

1.1 Filler distribution in rubber blends

The material used for tires, conveyor belts and other high-performance elastomer products needs to fulfill certain properties. Among the requirements for tires are the rolling resistance, the wet skid resistance and service life. Natural rubber has the highest durability due to strain-induced crystallization. This is reflected by the highest tensile strength and resistance to catastrophic crack growth [1,2]. SBR compounds show a good wet skid resistance, especially those with high styrene content [3]. Blending usually combines the properties of the individual polymers. But also synergetic effects are possible so that a blend can have a better property than both polymers [1,4,5]. Using polymer blends can result in a reduced compound cost, improve the building or the performance [6].

Communicated by Johlitz, Laiarinandrasana and Marco.

Matthias Wunde · Manfred Klüppel (✉)
Deutsches Institut für Kautschuktechnologie e. V. (DIK), 30519 Hannover, Germany
E-mail: Manfred.Klueppel@DIKautschuk.de

Besides on the components of the blend, the fracture mechanical properties depend on the distribution of the reinforcing filler into the different polymer phases [7]. Using master batches changes the filler distribution and can lead to enhanced reinforcement in silica-filled NR/BR/SBR blends [8]. The affinity of carbon black to NR and SBR in NR/SBR blends has been studied by several authors using different techniques [9–14], all of them detecting a higher affinity of the SBR to CB. The higher carbon black loading in the SBR phase is explained by stronger carbon black polymer interactions [9,10]. Le et al. [9] studied the kinetics of the filler distribution with thermogravimetry on the rubber–filler gel [9]. The NR bonds to the CB more quickly, but with increased mixing time the filler transfers to the SBR phase due to the stronger SBR-CB bonds. Cotton and Murphy [10] showed by analysis of bound rubber that the molecular weight of the polymers is affecting the carbon black dispersion. The carbon black affinity increases with higher molecular weight, but the effect is weak for the immiscible NR/SBR blends. Also, higher carbon black loadings in the SBR with increasing surface area of the carbon black and with increased mixing time are revealed. Other techniques applied to study the carbon black affinity include, phase contrast optical microscopy [11,12], inverse gas liquid chromatography [13], and combined measurements of the static and dynamic modulus [14]. Differences in the carbon black distribution measured by the different techniques are caused, not only but also, from different ingredients used in the compounds. The rubbers are not identical, e.g., varying in styrene content of the SBR and different molecular weights of the NR. The CB also differs in grade and content. The previously mentioned techniques do not state information about the interphase and the interphase filling. But both the magnitude of the interphase connecting different polymer phases and the filler amount in the interphase are influencing the fracture mechanical properties of the blend.

1.2 Evaluation of filler distribution based on viscoelastic spectra

By the evaluation of the increase in the loss modulus peaks, the filler distribution not only in the two polymer phases but also in the interphase can be obtained. A fitting procedure separating the contributions of the different polymer phases and also of the interphase to the temperature-dependent total dissipated energy G'' during dynamical straining is presented [15–19]. Due to the filler located in a specific phase, the energy dissipation in that phase is increased. From the increase of energy dissipation in the different phases, it is possible to determine the carbon black amount in the phases.

This method was already used to study the filler distribution in elastomer blends. The results of this study are within the range of previous results of NR/SBR blends using this technique [15–17]. All studies agree in a higher affinity of CB to SBR, but there are differences in the extent of the affinity toward the SBR. The differences may be caused by material variation. In NR/BR blends, contradictory results have been reported. A higher filling of the BR phase [15] as well a very low filling of the BR phase [18] were found. Also, studies on carbon black-filled EPDM/BR blends [15,16,20] and SBR/EPDM blends were performed [17]. Furthermore, silica-filled compounds have been studied [8,21,22].

1.3 Fracture mechanics of rubbers

Elastomer products made of NR/SBR blends like tires often need to sustain high dynamic loading conditions inducing crack propagation. Micro-mechanical mechanisms of crack initiation and propagation occurring under quasi-static and dynamic loading conditions are in current investigation [7]. The characteristics of crack initiation could be recently connected to the flaw size in the rubber [23,24]. Fracture mechanical methods and models for viscoelastic solids are based on the fundamental work of Rivlin and Thomas [25]. Although recent efforts have been made [26–29], there is still potential, especially due to the strongly nonlinear deformation behavior and stress softening effects [7,30,31]. The fracture mechanical properties of tires and conveyor belts can be characterized by the Fatigue Crack Growth and the Chip & Cut behavior of the rubber composites [32,33]. The Fatigue Crack Growth is at present usually carried out using the tear fatigue analyzer and evaluates the crack growth velocity under given loading conditions [34,35]. The Chip & Cut behavior is described by the tearing of rubber under harsh loading conditions that lead to a removal of rubber pieces. This effect is measured by the weight change in a rotating wheel dynamically impacted by a sharp tool [32,33,36].

Table 1 Recipes of the compounds (in phr)

Samples	NR	SBR	CB	CBS	Sulfur	IPPD	ZnO	Stearic acid
NR	100	–	50	2.5	1.7	1.5	3	1
N85S15	85	15	50	2.5	1.7	1.5	3	1
N70S30	70	30	50	2.5	1.7	1.5	3	1
N70S30Batch	70	30	50	2.5	1.7	1.5	3	1
N55S45	55	45	50	2.5	1.7	1.5	3	1
N55S45Batch	55	45	50	2.5	1.7	1.5	3	1

Batch denotes samples mixed with the batching mixing procedure (carbon black blended first in NR only)

2 Experimental

2.1 Materials

The investigation is carried out on polymer blends based on natural rubber (SVR CV 60) blended with styrene-butadiene rubber (Buna VSL 4526, Lanxess) with 45 wt% vinyl and 26 wt% styrene groups with varying proportion of the polymers. As filler, 50 phr (parts per hundred rubber) of carbon black (N339) are used. The samples are cross-linked semi-efficiently by sulfur and the vulcanization accelerator *N*-cyclohexyl-2-benzothiazole sulfonamide (CBS). The samples are compounded with the processing and vulcanization additives stearic acid and zinc oxide and protected against aging by *N*-isopropyl-*N*′-phenyl-*p*-phenylendiamine (IPPD). The full recipe is shown in Table 1.

2.2 Sample preparation

The compounds are mixed in an industrial 5-liter intermeshing mixer (Werner & Pfleiderer GK 5 E) at 40 rpm for 6 min. After 2-min mastication of the polymers, the other ingredients are inserted. The homogeneity of the mixtures is indicated by leveling of the torque after mastication and after mixing. The composites are handled another 7 min on a roller mill where the curing system is added. Vulcanization is performed at 150 °C in a heat press up to 90% of the vulcameter torque maximum (t_{90} time).

Two different mixing techniques are used. In the standard mixing procedure, the polymers are mixed first, and then, the filler is added. In the batch mixing procedure, the filler is first blended with the NR only and the SBR and the other ingredients are added in a second mixing stage. After the second mixing stage, the curing system is mixed in the roller mill.

2.3 Optical dispersion analysis

The carbon black dispersion is checked by optical dispersion analysis. As non-dispersed filler scatters the light diffusely, a computer-aided evaluation [Dispersions Index Analysis System (DIAS), developed at DIK] can determine the agglomerate size distribution of the filler from reflected-light microscope images. The images are taken on fresh elastomer surfaces at 150 times magnification. For each compound, five images are evaluated. The degree of dispersion is estimated by the portion of non-dispersed carbon black in the observed surface. In the estimation of dispersion grade, the medalia factor v representing the volume fraction of carbon black in the agglomerates is taken into account [37,38].

2.4 Dynamic-mechanical analysis

The dynamic-mechanical properties are measured in the torsion-rectangular mode on an ARES rheometer (Rheometrix) with strip specimen of 2 mm thickness. The dynamic moduli are measured over a wide temperature range (−90 to +20 °C) in steps of 1 °C at a frequency of 1 Hz and 0.5% strain amplitude.

2.5 Tear fatigue analyzer

The fracture mechanical measurements are performed on a tear fatigue analyzer (Coesfeld) at notched strip samples. This machine can detect the crack length of 10 specimens simultaneously. The crack propagation rates are measured under pulsed excitation (4 Hz, 30 ms pulse width) at 60 °C. The 15 mm broad samples with a 1-mm-deep crack are pre-strained by 2 N and excited by varying strain amplitudes between 10 and 30%. The graphical images for determination of the crack length are triggered between the pulses.

3 Viscoelastic response of filled rubber blends

3.1 Effect of fillers in homo-polymers

A single polymer shows a peak of the dissipated energy G''. The peak, centered around the glass transition temperature T_g of the polymer, is increased by filling with an active filler. Previous investigations have shown that the maximum of the dissipated energy G''_{max} increases almost linearly with the filler volume fraction ϕ_F [15,16,22]:

$$G''_{max}(\phi_F) = G''_{max,0} + \alpha\phi_F \tag{1}$$

Here, $G''_{max,0}$ is the maximum of the loss modulus of the unfilled polymer.

Storage and loss modulus G' and G'' are real and imaginary part of a complex function G^*, and both moduli have a connection analogous to Kramers–Kronig relations. This connection links the linear increase in the maximum of dissipated energy G''_{max} given in Eq. (1) with a linear increase in the step height of the storage modulus G'. The step height itself is dominated by the value of T_g in the glass, as G' in the rubber is 2–3 orders of magnitude lower (Fig. 1a). Accordingly, a similar linear relation as Eq. (1) holds for the storage modulus in the glassy regime:

$$G'_{glass}(\phi_F) = G'_{glass,0} + \alpha'\phi_F \tag{2}$$

with $\alpha' \approx \alpha$. Here, G'_{glass} is the storage modulus of the filled rubber in the glass and $G'_{glass,0}$ is the storage modulus of the unfilled rubber in the glass. In Fig. 1b, the linear increase in G''_{max} and in G' at −90 °C is shown. Above the glass transition, hydrodynamic amplification plays a role and an additional quadratic term enters, presuming very stiff filler compared to the stiffness of the polymer [39]. In Fig. 1b, no quadratic behavior can be seen for the NR, while for the SBR a very small quadratic term is possible. The linearity in Fig. 1b valid for NR/SBR blends seems to be a general characteristic in the glassy regime where the stiffness of the filler and the polymer is in the same order [15–17,20,22].

Ziegler and Schuster [22] studied the influence of silanization in BR and NBR on the slope of G'' with the filler volume fraction ϕ_F. They found that the front factor α of Eq. (1) increases systematically with the rubber–filler interaction strength. The polar silica interacts strongly with the polar NBR but only weakly with the non-polar BR. The silanization decreases the polarity of the silica surface and the intensity of rubber–filler interactions with the NBR decreases but with the BR increases. The change in the strength of interactions correlates with a decrease in the slope of $G''(\phi_F)$ in NBR and an increase in the slope in BR.

A linear dependency of G' in the glass can be explained by a parallel coupling of the pure rubber and of the rubber–filler structures consisting of the filler network including strongly bounded, immobilized rubber:

$$G'_{glass}(\phi_F) = (1 - \phi_F)G'_{glass,0} + \phi_F G'_{CB} \tag{2'}$$

This parallel coupling requires that the strain of both components is almost the same. The storage modulus of the rubber–filler structures at −90 °C yields $G'_{CB} = 2260$ MPa for NR and $G'_{CB} = 2480$ MPa for SBR, indicating that the rubber–filler structure of NR is softer than that of SBR. This can be related to (immobilized) polymer bridges between the filler particles that transmit the stress similar as in the rubber elastic regime well above T_g [39,40].

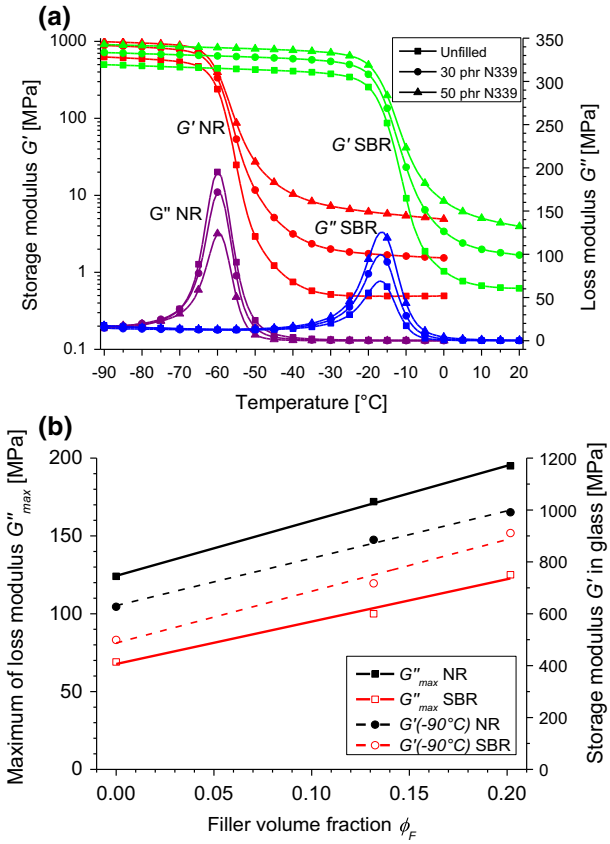

Fig. 1 Temperature-dependent moduli G' (logarithmic scale) and G'' for unfilled and differently filled NR and SBR compounds (**a**). Linear increase in the maximum loss modulus $G''_{\max}$ and of the storage modulus G' in the glass at −90 °C with filler volume fraction ϕ_F in NR and SBR, respectively (**b**)

3.2 Phase network of unfilled blends

The mechanical response of the phase network of unfilled blend systems with one phase glassy and the other not, can be described by percolation theory [15]. In percolation theory, there exists a critical concentration ϕ_c, at which the initially separated domains grow together to form an infinite cluster. Then, the largest phase domain of the glassy polymer becomes infinite large, leading to a phase transition at ϕ_c [41]. ϕ_c depends on the assumed lattice structure. The correlation length ξ for this polymers is given by the mean distance between two sites on the same polymer domain for polymer concentrations $\phi < \phi_c$ and between two empty sites of the same hole (corresponding to two sites on the same domain of the other polymer) for $\phi > \phi_c$, respectively. When ϕ is approaching the threshold ϕ_c, the correlation length increases as:

$$\xi \cong a\,|\phi - \phi_c|^{-\nu} \tag{3}$$

with the same exponent ν below and above ϕ_c. Here, a is the characteristic size of the domains [41]. The situation below and above the threshold ϕ_c is exemplified on phase contrasted TEM images of EPDM/NR blends (Fig. 2). Images of this blend show better contrast than NR/SBR blends due to staining by osmium tetraoxide so that the bright dispersed EPDM phase below ϕ_c and the interpenetrating phase network above ϕ_c can be seen.

Other quantities associated with the percolation transition show a similar power-law behavior with other critical exponents. The storage modulus of the glassy phase is given by:

$$G'_{\text{glass}} \cong E\left(\frac{a}{\xi}\right)^3 / N_1(\xi) \tag{4}$$

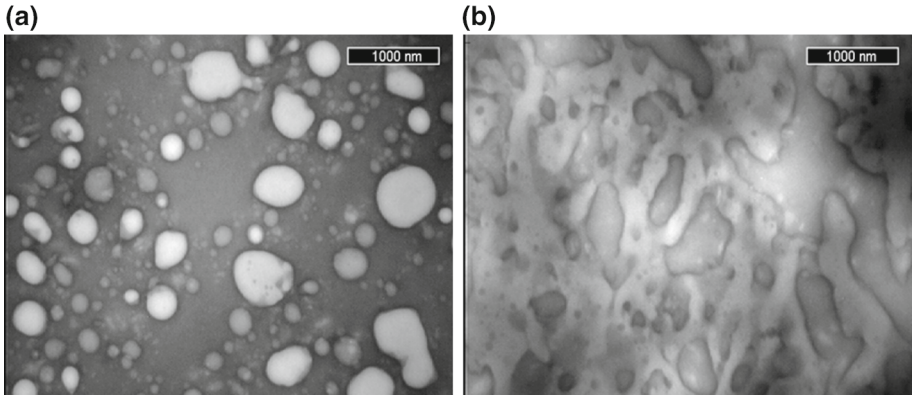

Fig. 2 Phase morphology of phase-contrasted EPDM/NR blends: dispersed phase morphology of the EPDM/NR (20:80) blend (**a**) and interpenetrating phase network in the EPDM/NR (60:40) blend (**b**)

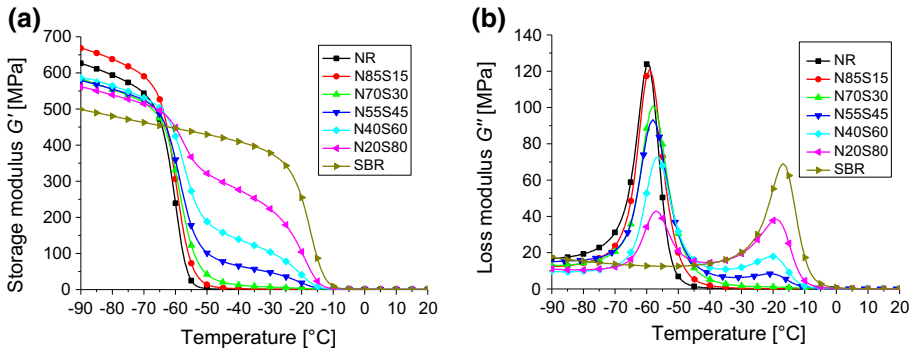

Fig. 3 Storage modulus G' (**a**) and loss modulus G'' (**b**) of unfilled NR/SBR blends

where E is the elastic modulus of the glassy phase and $N_1(\xi)$ is the number of singly connected bonds of the phase network. With Eq. (3) and $N_1(\xi) = \left(\frac{\xi}{a}\right)^{\frac{1}{\nu}}$ [15,41], it follows:

$$G'_{\text{glass}} \cong E\,(\phi - \phi_c)^{3\nu+1} \sim (\phi - \phi_c)^{\tau} \tag{5}$$

The shear modulus G' of the polymer phase increases above ϕ_c with the critical exponent $\tau = 3\nu + 1 \approx 3.6$ [42]. The exponents ν and τ are universal and do not depend on details of the percolation [15]. Based on this approach, the filler network and the Payne effect have also been described [43].

When the temperature in an unfilled blend is chosen in-between both glass transition temperatures, the elastic modulus is dominated by the harder glassy phase, when this phase is above the threshold ϕ_c [15]. Below ϕ_c, the glassy domains remain undeformed during dynamic excitation because of their large modulus compared to that of the continuous NR. Then, the glassy domains of the SBR enhance the modulus only by hydrodynamic amplification. Above the percolation threshold, the glassy domains of the SBR form a continuous phase network, where most energy is stored. The percolation behavior of the glassy SBR phase is shown in Fig. 3 for the NR/SBR blends in the temperature range around −40 °C. Below the threshold ϕ_c, the storage modulus G' shown in Fig. 3a at temperatures around −40 °C is very small and increases substantially above ϕ_c. An analogous increase can be seen for the local maximum of the loss modulus G'' in Fig. 3b.

Figure 4a shows a fit of G' at different temperatures in-between both glass transitions and of G''_{max} according to the power law Eq. (5) for different SBR contents above the critical SBR concentration ϕ_c. The value of $\phi_c = 0.22$ has been fitted to get a minimum variance. The slope is found as $\tau = 1.34$ for $G'(-45\,°\text{C})$, $\tau = 1.53$ for $G'(-40\,°\text{C})$, $\tau = 1.65$ for $G'(-35\,°\text{C})$, $\tau = 1.73$ for $G'(-30\,°\text{C})$ and $\tau = 1.76$ for G''_{max}. This differs significantly from the theoretical value $\tau \approx 3.6$, which can be related to coalescence effects that alter the phase network structure.

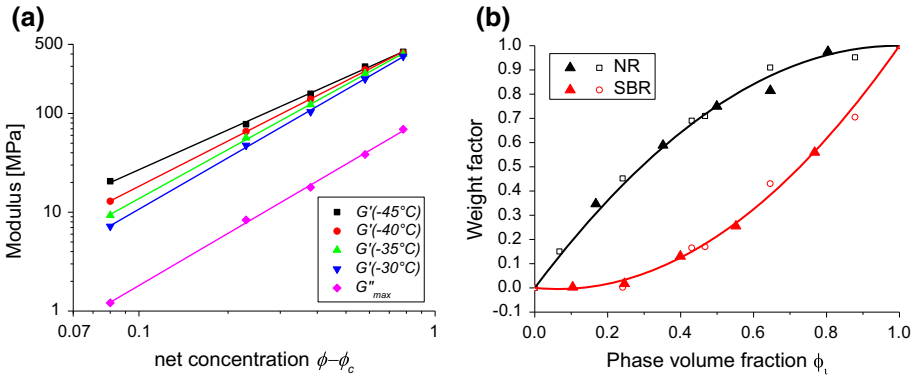

Fig. 4 Increase in the storage modulus of unfilled NR/SBR blends at temperatures between −45 and −30 °C and the maximum of the loss modulus with increasing SBR content. A power-law behavior according to Eq. 5 above $\phi_c = 0.22$ can be identified (**a**). Weight factor $G''_{\text{max,blend}}/G''_{\text{max,polymer}}$ (**b**). The *open symbols* represent data taken from Schuster et al. [16]. The *full triangles*, indicating own data, fit well with the previous data. All values are fitted by Eq. 7

3.3 Energy dissipation in filled rubber blends

The total dissipated energy G''_{blend} is due to the additivity of energy the sum of all energy contributions of the different phases i:

$$G''_{\text{blend}} = \sum_i G''_{\text{P},i}\phi_i\gamma_{0,i}^2 \tag{6}$$

$G''_{\text{P},i}$ denotes the loss modulus, ϕ_i the volume fraction and $\gamma_{0,i}$ the strain amplitude of the ith phase.

In an unfilled blend, the dissipated energies of the phases depend nonlinearly on their phase volume fractions. The weight factors in term of their volume fractions are fitted by quadratic functions (Fig. 4b):

$$G''_{\text{blend}} = \sum_i G''_{\text{P},i}\left(a_i + b_i\phi_i + c_i\phi_i^2\right) \tag{7}$$

The quadratic increase in the weight factor of the SBR in Fig. 4b correlates with the power law increase with linear slope of the log-log plot of G''_{max} in Fig. 4a.

In incompatible polymer blends, each polymer phase causes dissipation around its glass transition temperature. Besides the NR and the SBR phase, areas exist in which both polymers coexist. This so-called interphase leads to an enhanced signal of G'' between the pure polymer peaks. The dissipated energy in unfilled, as well as filled blends, can be decomposed into the contributions from the different phases and the interphase. For this decomposition, a fitting routine is used. The amplitude and broadness of the peaks as well as the glass transition temperature are used as fitting parameters. The increase in the peaks with increasing filler content is due to the specific filler loading of the phases.

For the unfilled blends, the dynamic spectrum is fitted with the unfilled NR and SBR peaks so that the sum of both contributions coincides best with the measured curve in the two areas around both glass transition temperatures (Fig. 5). The interphase signal is received as the difference between the viscoelastic spectrum of the unfilled blend compared to the sum of the unfilled polymers.

In a filled blend, the filler effect (Eq. (1)) and the blend effect (Eq. (7)) are combined. The filler located in any phase (or the interphase) increases the dissipated energy of that phase. From the increase in the maximum of the dissipated energies G''_{max} in the different phases and the interphase, the filler volume fractions $\phi_{\text{F},i}$ of the different phases i can be calculated:

$$G''_{\text{blend}} = \sum_i \left(1 + \alpha_i \frac{\phi_{\text{F},i}}{\phi_{\text{F},i} + \phi_i}\right)\left(a_i + b_i\left(\phi_{\text{F},i} + \phi_i\right) + c_i\left(\phi_{\text{F},i} + \phi_i\right)^2\right) G''_{\text{P},i} \tag{8}$$

The dynamic spectra of the filled blends are fitted with the unfilled NR and SBR peaks and the interphase peak so that the sum of all three curves corresponds best with the measurements (Fig. 6). The filler volume fractions in the phases and interphases $\phi_{\text{F},i}$ are obtained from the increase in the maximum values of G'' using Eq. (8).

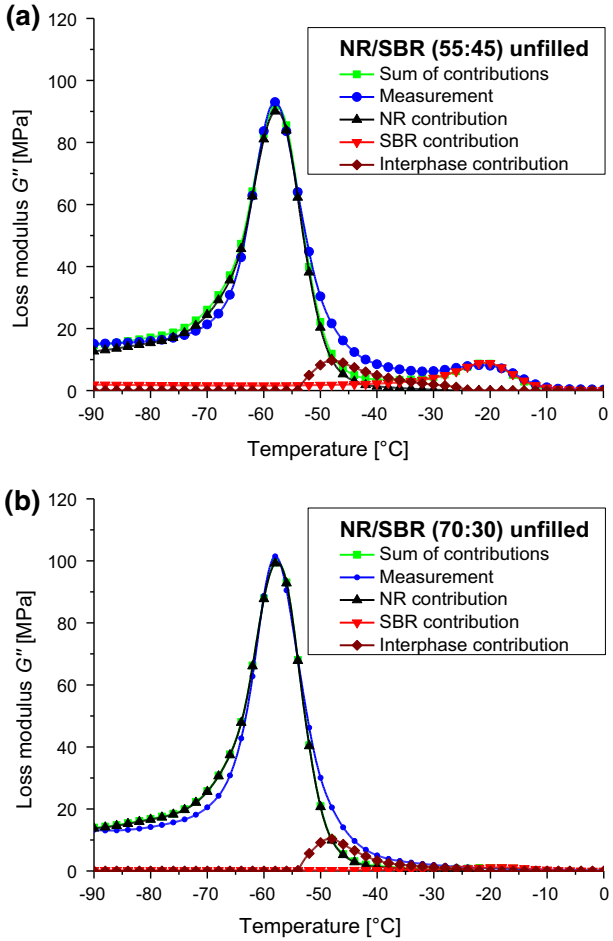

Fig. 5 Fit of the loss modulus of the unfilled NR/SBR blends with the single polymer peaks. The interphase is obtained as fit difference: unfilled NR/SBR (55:45) blend (**a**) and unfilled NR/SBR (70:30) blend (**b**)

When calculating the filler volume fractions $\phi_{\mathrm{F},i}$ with Eq. (8), there is no intrinsic reason why the calculated sum $\sum_i \phi_{\mathrm{F},i}$ should exactly match the overall filler concentration ϕ_{F}. Therefore, the sum of the calculated filler has a standard deviation of about 10% from the filler content in the samples. Nevertheless, all compounds should contain the same filler amount $\phi_{\mathrm{F}} = 0.2017$. That is why for every compound the filler volume fraction is corrected by a factor around 1 so that

$$\sum_i \phi_{\mathrm{F},i} = \phi_{\mathrm{F}} \tag{9}$$

is fulfilled. If the correction factor deviates strongly from unity, it is a sign for unreliable results and the reasons for that should be understood. For the compound with only 15 phr SBR, the dynamic spectrum is dominated by the NR peak. The very small SBR peak of the unfilled compound does not allow a reliable calculation of the filler volume fraction $\phi_{\mathrm{F},S}$ in the filled sample.

4 Phase morphology of filled blends

4.1 Carbon black distribution

Figure 7 shows the calculated carbon black distribution in the NR/SBR blends. A higher filling of the SBR phase and the interphase is found, while the NR phase is lower filled. These results are obtained for all blends with varying proportion of the polymers.

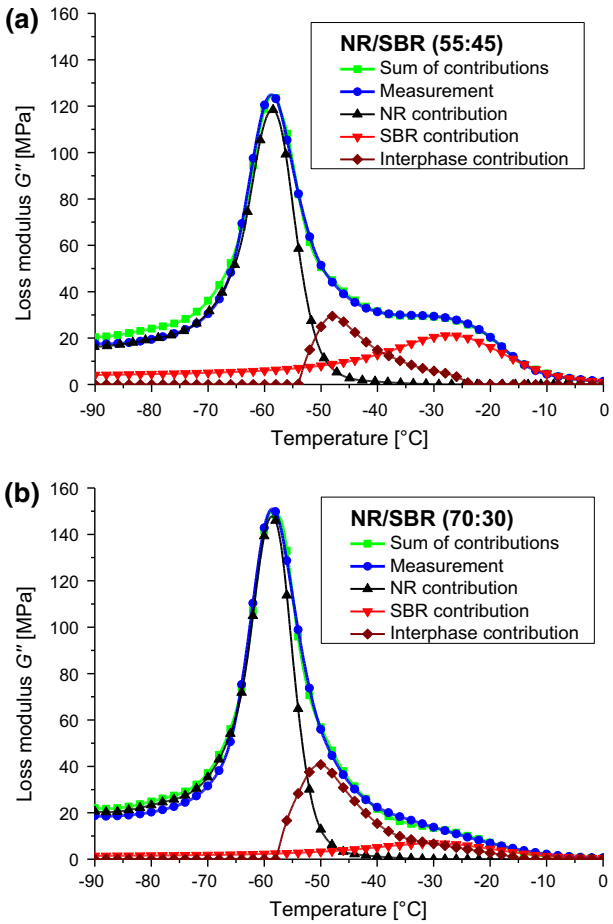

Fig. 6 Fit of the loss modulus of the filled NR/SBR blends with the single polymers and the interphase. The filling of the phases and the interphase is obtained from the increase in the maxima of the contributions using Eq. (7): filled NR/SBR (55:45) blend (**a**) and filled NR/SBR (70:30) blend (**b**)

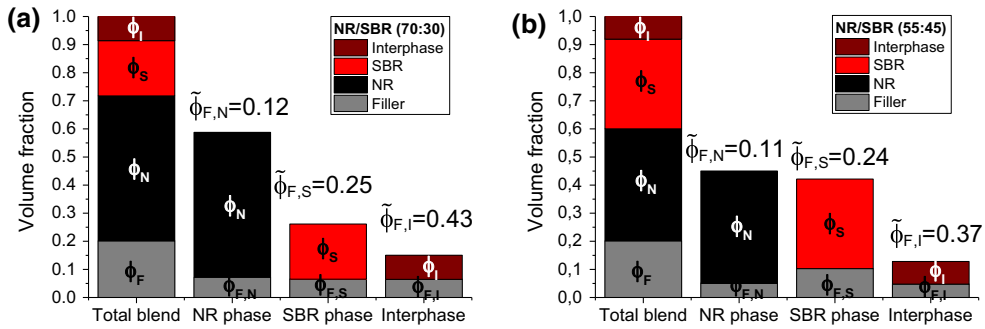

Fig. 7 Carbon black distribution in NR/SBR blends: NR/SBR (70:30) (**a**) and NR/SBR (55:45) (**b**) (from Ref. [18]). $\tilde{\phi}_{F,i}$ denotes the relative filler volume fraction in phase i

Figure 8 shows the carbon black distribution in the NR/SBR blends mixed with the batching mixing procedure. In the batch, the whole amount of filler is mixed into the NR, but as the SBR has the higher affinity to carbon black, the filler needs to transfer from the NR to the SBR phase. Because of this transfer, more carbon black gets stuck in the interphase, leading to a higher filling of the interphase compared to the standard mixing procedure. Batching also seems to lead to a slightly higher filling of the NR phase and a lower filling of the SBR phase.

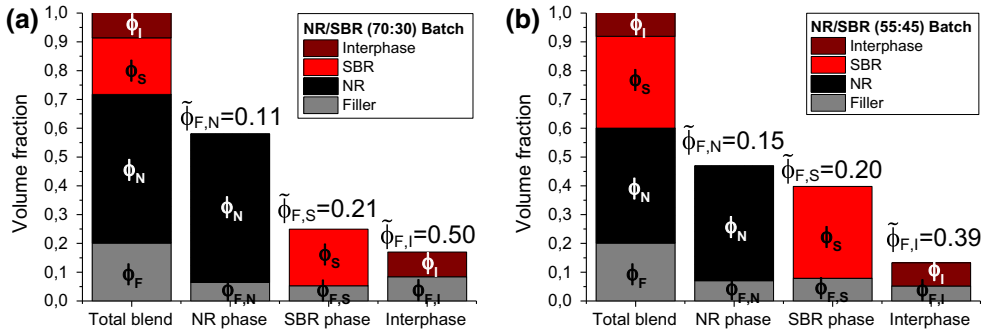

Fig. 8 Carbon black distribution in NR/SBR blends mixed with the batch mixing procedure (CB first mixed into NR only): NR/SBR (70:30) batch (**a**) and NR/SBR (55:45) batch (**b**). $\tilde{\phi}_{F,i}$ denotes the relative filler volume fraction in phase i

Table 2 Proportion of carbon black $\tilde{\phi}_{F,i} = \phi_{F,i}/(\phi_i + \phi_{F,i})$ of the different phases in the NR/SBR blends

Filler volume fraction	N70S30	N70S30 Batch	N55S45	N55S45 Batch
$\tilde{\phi}_{F,N}$	0.12	0.11	0.11	0.15
$\tilde{\phi}_{F,S}$	0.25	0.21	0.24	0.20
$\tilde{\phi}_{F,I}$	0.43	0.50	0.37	0.39

Table 3 Ratio $\phi_{F,i}/\phi_F$ of the carbon black distributed into the different phases of the NR/SBR blends

Carbon black portion in	N70S30 (%)	N70S30 Batch (%)	N55S45 (%)	N55S45 Batch (%)
NR phase	36	32	26	35
SBR phase	32	26	51	39
Interphase	32	42	24	26

Table 2 summarizes what proportion of the different phases and the interphase consists of carbon black. The filler volume fractions in the NR $\tilde{\phi}_{F,N}$ as well as in the interphase $\tilde{\phi}_{F,I}$ seem to increase slightly with increasing NR content in the blend, while the proportion of the SBR seem to stay constant. It is no contradiction that no proportion is falling because the amount of the lowly filled NR phase is obviously rising with NR content.

In Table 3, it is shown how much of the filler is distributed in the different phases and the interphase. Due to its higher volume fraction $\phi_{F,N}$, a significant amount of the filler is found in the NR phase, although it is low filled. The interplay between carbon black affinity and the amount of the specific phases leads for many of the studied compounds to filler distributions with similar amount of carbon black in the different phases and interphases.

The proportions given in Table 3 can be compared with literature data. Cotten and Murphy [10] discovered for a similar 50:50 blend that 31.1% of the carbon black is found in the SBR phase and 58.9% in the NR phase. The SBR used is also solution polymerized with similar amount of 25% styrene. The compounds are filled with 45 phr of the same carbon black N339. When considering that they did not distinguish the carbon black located in the interphase, both results fit fairly well. Callan et al. [14] detected in a NR/SBR 50:50 blend using emulsion SBR, an even higher carbon black loading in the SBR. Also, other studies measured a preferred carbon black affinity of the SBR, but did not quantify the filler distribution in the blends [12,13]. Previous measurements using our technique on NR/SBR blends have been made: In a 50:50 blends containing a solution SBR with 25% styrene and 60 phr N234, 51% of the filler is found in the SBR and 12 and 37% are found in the NR phase and interphase, respectively [17]. That is a lower NR filling and a higher interphase filling. In a 70:30 blend using a solution SBR with 40% styrene, a higher carbon black amount in the NR and a lower amount in the interphase is found [15]. On the contrary for NR/SBR (40:60) blends, a lower NR filling and a higher interphase filling are found [16]. When studying the filler distribution of NR/SBR blends using different techniques, the preference of the carbon black to the SBR is clearly resulting. But even using a single technique, the quantitative filler distribution seems to be strongly influenced by material variation. Also, the mixing is influencing the filler distribution as can be seen by comparing the results for the standard and the batch mixing procedure.

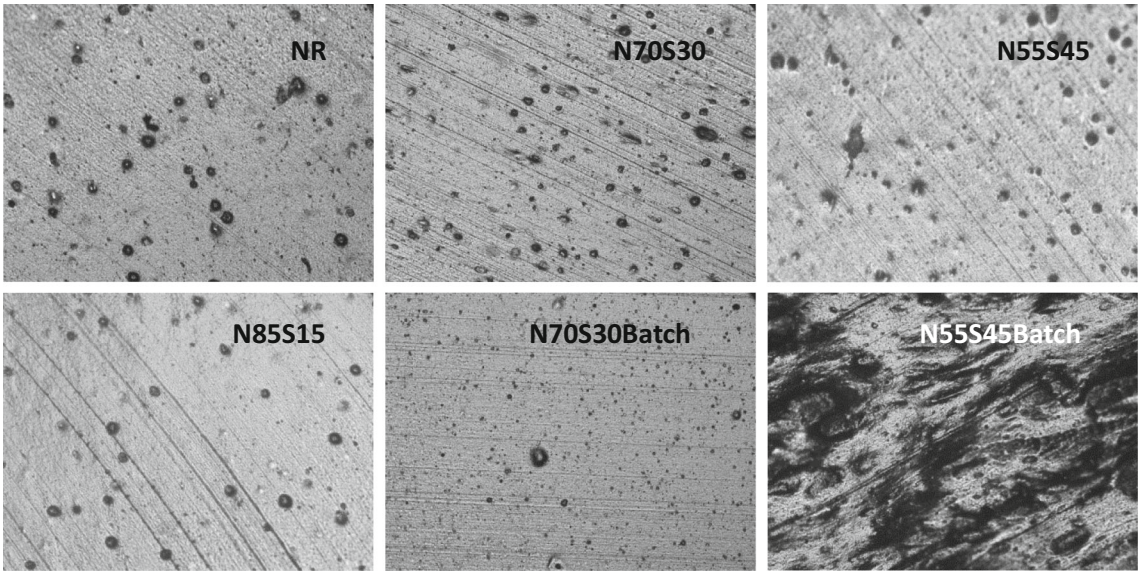

Fig. 9 Exemplary optical dispersion images of the compounds

4.2 Optical dispersion analysis

In Fig. 9, images for different compounds are shown. In the images, not dispersed filler is appearing dark because the light is scattered diffusely. All compounds show a good dispersion of around 90%. Only the compound with 55 phr NR mixed with the batch mixing technique N55S45Batch has a very bad dispersion. In this mixture, 50 phr CB need to be premixed in only 55 phr NR. This is equivalent to a compound with 91 phr CB. Therefore, the carbon black could not be incorporated well. Also, in the second mixing step after addition of the SBR no good dispersion could be achieved.

5 Fracture mechanical properties

5.1 Evaluation of tearing energy and crack propagation rates

The energy dS needed to increase crack surfaces cannot exceed the release of elastic energy $-\mathrm{d}W$ (Griffith criteria) [44]. The elastic energy release rate $T = -\mathrm{d}W/\mathrm{d}S$ is called tearing energy. The tearing energy regulates the crack propagation under fixed conditions. Using the tear fatigue analyzer, the tearing energy is adjusted by the strain preset (and slightly by the initial crack length). The crack propagation rate per cycle $\mathrm{d}c/\mathrm{d}n$ in dependence of T is characterized by the power law from Paris and Erdogan [45,46]:

$$\frac{\mathrm{d}c}{\mathrm{d}n} = AT^B \tag{10}$$

The Paris–Erdogan law is applied to the tear fatigue measurements. Therefore, the crack contour length $c_{contour}$ is evaluated in a region of stable crack growth. The crack contour length is in contrast to the crack depth x directly related to the crack surface and therefore to the tearing energy. For some samples, a second stable region is evaluated. The crack growth rate $\mathrm{d}c/\mathrm{d}n$ is obtained as the slope in the stable regions. The tearing energy of a single-edge notched (SEN) strip sample is given by [17]:

$$T = \frac{2\pi}{\sqrt{\langle\lambda\rangle}}\langle w_{\mathrm{el}}\rangle\langle c\rangle \tag{11}$$

where $\langle\lambda\rangle$ is the average elongation and $\langle w_{\mathrm{el}}\rangle$ is the average elastic energy density. Equation (11) is no exact formula. FEM simulations [47] show that the linear dependency on crack length is valid only for crack depths smaller than 20% of the sample width. However, the error for crack lengths substantially longer is small. Lorenz et al. [17] showed that Eq. (11) can be used to describe $c(n)$ even up to crack depths of 40% of the

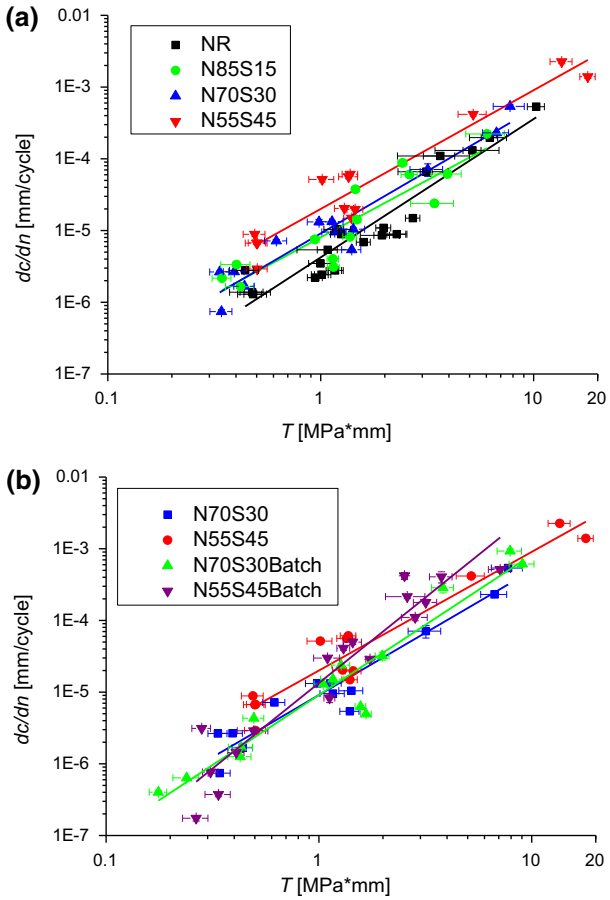

Fig. 10 Crack propagation per cycle $\mathrm{d}c/\mathrm{d}n$ versus tearing energy T for **a** NR/SBR blends (standard mixing procedure) and **b** NR/SBR blends (standard vs. batch mixing procedure)

sample width provided the crack remains perpendicular to the stretching direction and does not turn. T is calculated with the elastic density relating to the cross-sectional area, $w_{\mathrm{el,Rest}}$.

Because filled rubbers show strong nonlinear behavior and hysteresis, energy is not only dissipated at the process zone at the crack tip but also far away from the crack tip. In fact, the crack growth does not depend on the global tearing energy T but on the energy available at the process zone. This energy can be evaluated using the concept of J-integral. By the J-integral

$$J = \int_{\Gamma} (W * \vec{n} - \bar{\bar{\sigma}} * \vec{n} * \nabla \vec{u}) \tag{12}$$

the energy flow into a small volume around the crack tip can be accessed. Here, Γ is a path surrounding that volume, $\vec{n}$ is the normal vector of that path, W is the energy density, $\bar{\bar{\sigma}}$ is the stress tensor and $\nabla \vec{u}$ is the displacement gradient. An investigation dealing with the analytic determination of the J-integral based on an advanced material model was recently proposed [48]. Here, we will use Eq. (11) for the evaluation of the tearing energy.

5.2 Crack propagation under pulsed loading

Figure 10a shows the fracture mechanical properties of the NR/SBR blends prepared by normal mixing. The crack propagation of NR/SBR blends increases slightly, but in clear order, with increasing SBR content. The crack growth rate at fixed tearing energy increases almost linearly with the SBR content. The compounds N70S30 and N70S30Batch, with 70 phr NR and 30 phr SBR, show a similar crack growth behavior with a

slightly worse crack growth resistance of the batch at high tearing energies (Fig. 10b). This is possibly related to the higher filler loading of the interphase accompanied by the lower filling of the SBR phase (compare Figs. 7, 8). However, the differences of the two compounds in the NR loading as well as in the crack growth results are within the error range of the measurements. The differences in the carbon black distribution of the compounds N55S45 and N55S45Batch, with 55 phr NR and 45 phr SBR, are as expected. In the batch compound, in which all filler is mixed with the NR first, more filler is found in the NR phase and in the interphase and less filler is detected in the SBR. As shown in Fig. 9, the compound N55S45Batch has a very bad dispersion. The bad dispersion is expected to be responsible for the higher slope in the Paris–Erdogan plot, and the influence of dispersion is covering possible effects due to the difference in filler distribution.

6 Conclusions

The carbon black distribution into the different phases and interphases of NR/SBR blends has been analyzed by referring to a viscoelastic model of energy dissipation in the glass transition process. Throughout the entire study, the SBR shows a higher carbon black affinity than the NR. The filler amount calculated lies midway in the literature data and quite close to data for similar compounds [9–14]. But in contrast to other techniques also statements about the interphase are possible. A high interphase filling for all compounds is found. By the batch mixing procedure of the NR/SBR blend a higher interphase filling and a lower SBR filling is obtained. Crack propagation rates increase slightly with increasing SBR content. The effect of batch mixing procedure on filler distribution was analyzed delivering a higher filling of the interphase and lower filling of the SBR phase. The crack propagation rates are slightly increased for the batched sample with 70% NR and 30% SBR (N70S30Batch). The crack propagation of the N55S45Batch sample, with 55% NR and 45% SBR prepared by batch mixing, is worse at high tearing energies which probably results from the bad carbon black dispersion.

Acknowledgements We thank the Deutsche Forschungsgemeinschaft (DFG) for financial support (Grant No. KL1409/9-1) and our project partners IPF Dresden and Continental AG for the very fruitful cooperation.

References

1. Kim, H.J., Hamed, G.R.: On the reason that passenger tire sidewalls are based on blends of natural rubber and *cis*-polybutadiene. Rubber Chem. Technol. **73**, 743 (2000)
2. Hamed, G.R., Kim, H.J., Gent, A.N.: Cut growth in vulkanizates of natural rubber, *cis*-polybutadiene, and a 50/50 blend during single and repeated extension. Rubber Chem. Technol. **69**, 807 (1996)
3. Takino, H., Nakayama, R., Yamada, Y.: Viscoelastic properties of elastomers and tire wet skid resistance. Rubber Chem. Technol. **70**, 584 (1997)
4. Clapson, B.E., Lake, G.J.: Truck tire groove cracking theory and practice. Rubber J. **152**, 36 (1970)
5. Mangaraj, D.: Elastomer blends. Rubber Chem. Technol. **75**, 365 (2002)
6. Hess, W.M., Herd, C.R., Vegvari, P.C.: Characterization of immiscible elastomer blends. Rubber Chem. Technol. **66**, 329 (1993)
7. Gent, A.N.: Engineering with rubber. Hanser, Munich (2001)
8. Meier, J.G., Klüppel, M., Geisler, H., Schuster, R.H.: Kieselsäuregefüllte Elastomerblends durch Masterbatchtechnologie. Kautsch. Gummi Kunstst. **58**, 587 (2005)
9. Le, H.H., Ilisch, S., Kasaliwal, G.R., Radusch, H.-J.: Thermogravimetrischer Analyse an Kautschuk-Füllstoff-Gel: Bestimmung der phasenspezifischen Füllstoffverteilung in Kautschukblends. Kautsch. Gummi Kunstst. **60**, 241 (2007)
10. Cotten, G.R., Murphy, L.J.: Mixing of carbon black with rubber. VI. Analysis of NR/SBR blends. Rubber Chem. Technol. **61**, 609 (1988)
11. Hess, W.M., Scott, C.E., Callan, J.E.: Carbon black distribution in elastomer blends. Rubber Chem. Technol. **40**, 371 (1967)
12. Ayala, J.A., Hess, W.M., Kistler, F.D., Joyce, G.A.: Carbon-black–elastomer interaction. Rubber Chem. Technol. **64**, 19 (1991)
13. Schuster, R.H., Issel, H.M., Peterseim, V.: Selective interactions in elastomers, a base for compatibility and polymer–filler interactions. Rubber Chem. Technol. **69**, 769 (1996)
14. Callan, J.E., Hess, W.M., Scott, C.E.: Elastomer blends. Compatibility and relative response to fillers. Rubber Chem. Technol. **44**, 814 (1971)
15. Klüppel, M., Schuster, R.H., Schaper, J.: Carbon black distribution in rubber blends: a dynamic-mechanical analysis. Rubber Chem. Technol. **72**, 91 (1999)
16. Schuster, R.H., Meier, J., Klüppel, M.: The role of interphase in filler partition in rubber blends. Kautsch. Gummi Kunstst. **53**, 663 (2000)
17. Lorenz, H., Steinhauser, D., Klüppel, M.: Morphology and micro-mechanics of filled elastomer blends: impact on dynamic crack propagation. Lect. Notes Appl. Comput. Mech. **70**, 81 (2013)
18. Wunde, M., Klüppel, M.: Influence of phase morphology and filler distribution in NR/BR and NR/SBR blends on fracture mechanical properties. Rubber Chem. Technol. **89**, 588 (2016)

19. Wunde, M., Klüppel, M.: Carbon black distribution in blends of natural rubber with polybutadiene rubber and styrene-butadiene rubber. In: Proceedings of the14th International Seminar on Elastomers, Bratislava, Slovakia, Aug 24–28, p. 68. Librix.eu, Bratislava (2014)
20. Klüppel, M., Schuster, R.H., Schaper, J.: Dynamischer Glasübergang in füllstoffverstärkten Kautschukblends. GAK Gummi Fasern Kunststoffe **51**, 508 (1998)
21. Meier, J.F., Klüppel, M., Schuster, R.H.: Steuerung der physikalischen Eigenschaften von Elastomeren. Kautsch. Gummi Kunstst. **58**, 82 (2005)
22. Ziegler, J., Schuster, R.H.: Dynamisch-mechanische Eigenschaften und Verteilung von Kieselsäure in NBR/BR-Verschnitten. Kautsch. Gummi Kunstst. **56**, 159 (2003)
23. Huneau, B., Masquelier, I., Marco, Y., Le Saux, V., Noizet, S., Schiel, C., Charrier, P.: Fatigue crack initiation in a carbon black-filled natural rubber. Rubber Chem. Technol. **89**, 126 (2016)
24. Ludwig, M., Alshuth, T., El Yaagoubi, M., Juhre, D.: Lifetime prediction of elastomers based on statistical occurence of material defects. In: Marvalová, B., Petríková, I. (eds.) Constitutive Models for Rubber IX, pp. 445–448. Taylor & Francis, London (2015)
25. Rivlin, R.S., Thomas, A.G.: Rupture of rubber. I. Characteristic energy for tearing. J. Polym. Sci. **10**, 291 (1953)
26. Persson, B.N.J., Ahlbor, O., Heinrich, G., Ueba, H.: Crack propagation in rubber-like materials. J. Phys. Cond. Matter. **17**, R1071 (2005)
27. Persson, B.N.J., Brener, E.A.: Crack propagation in viscoelastic solids. Phys. Rev. E **71**, 036123 (2005)
28. Klüppel, M.: Evaluation of viscoelastic master curves of filled elastomers and applications to fracture mechanics. J. Phys Cond. Matter **21**, 035104 (2009). (10pp)
29. Reinke, K., Grellmann, W., Klüppel, M.: Investigation of fracture mechanical properties of filler-reinforced styrene-butadiene elastomers. Kautsch. Gummi Kunstst. **62**, 246 (2009)
30. Payne, A.R.: The dynamic properties of carbon black-loaded natural rubber vulcanizates. Part I. Rubber Chem. Technol. **36**, 432 (1963)
31. Ferry, J.D.: Viscoelastic Properties of Polymers, 3rd edn. Wiley, New York (1980)
32. Stocek, R., Kipscholl, R., Euchler, E., Heinrich, G.: Study of the relationsship between fatigue crack growth and dynamic chip & cut behaviour of reinforced rubber materials. Kautsch. Gummi Kunstst. **4**, 26 (2014)
33. Stocek, R., Ghosh, P., Mukhopadhyay, R., Kipscholl, R., Heinrich, G.: Fracture behaviour of rubber-like materials under classical fatigue crack growth vs. chip & cut analysis. In: Gil-Negrete, N., Alonso, A. (eds.) Constitutive Models for Rubber VIII, pp. 323–328. Taylor & Francis, London (2013)
34. Eisele, U., Kelbch, S.A., Engels, H.-W.: The tear analyzer—a new tool for quantitative measurements of the dynamic crack growth of elastomers. Kautsch. Gummi Kunstst. **1992**, 45 (1064)
35. Stocek, R., Heinrich, G., Gehde, M., Kipscholl, R.: Analysis of dynamic crack propagation in elastomers by simultaneous tensile- and pure-shear-mode testing. Lect. Notes Appl. Comput. Mech. **70**, 269 (2013)
36. Beatty, J.R., Miksch, B.J.: A laboratory cutting and chipping tester for evaluating off-the-road and heavy-duty tire treads. Rubber Chem. Technol. **55**, 1531 (1982)
37. Medalia, A.I.: Microscopic estimation of carbon black dispersion. Rubber Age **97**, 82 (1965)
38. Medalia, A.I.: Dispersion of carbon black in rubber: revised calculation procedure. Rubber Chem. Technol. **34**, 1134 (1961)
39. Vilgis, T.A., Heinrich, G., Klüppel, M.: Hydrodynamic reinforcement of elastomers. Reinforcement of Polymer Nano-Composites, Chapter 8
40. Klüppel, M.: The role of disorder in filler reinforcement of elastomers on various length scales. Adv. Polym. Sci. **164**, 1–86 (2003)
41. Bunde, A., Havlin, S. (eds.): Fractals and Disordered Systems, 2nd edn. Springer, Berlin (1996)
42. Kantor, Y., Webman, I.: Elastic properties of random percolating systems. Phys. Rev. Lett. **52**(21), 1891 (1984)
43. Lin, C.-R., Lee, Y.-D.: Strain-dependent dynamic properties of filled rubber network systems. Macromol. Theory Simul. **5**, 1075–1104 (1996)
44. Griffith, A.A.: The phenomena of rupture and flow in solids. Philos. Trans. R. Soc. Lond. A **221**, 163 (1921)
45. Paris, P.C., Gomez, M.P., Anderson, W.E.: A rational analytic theory of failure. Trend Eng. **13**, 9 (1961)
46. Paris, P., Erdogan, F.: A critical analysis of crack propagation laws. J. Basic Eng. **85**, 528 (1963)
47. Timbrell, C., Wiehahn, M., Cook, G., Muhr, A.H.: Simulation of crack propagation in rubber. In: Busfield, J.J.C., Muhr, A.H. (eds.) Constitutive Models for Rubber III, pp. 11–20. Swets Zeitlinger, Lisse (2003)
48. Wunde, M., Plagge, J., Klüppel, M.: Tearing energy in filler reinforced elastomers for tire treads. In: Proceedings, 12th Rubber Fall Colloquium, Hannover, Germany, Nov 22–24 (2016)